ACS OMEGA

Open Access

http://pubs.acs.org/journal/acsodf

Article

Chemical, Pharmacological, and Theoretical Aspects of Some Transition Metal(II) Complexes Derived from Pyrrole Azine Schiff Base

Sivan Arulmozhi, Gopalakrishnan Sasikumar, Annadurai Subramani,* Mustafa K. A. Mohammed,* Syed J. Askar Ali,* Sasikumar Ponnusamy,* Majid S. Jabir, Abdallah M. Elgorban, Wanli Zhang, and Hema Natarajan

Cite This: *ACS Omega* 2023, 8, 34458−34470

Read Online

ACCESS | Metrics & More | Article Recommendations | Supporting Information

ABSTRACT: Some new transition metal complexes were prepared by reacting metal(II) salts with Schiff base azines, which were prepared via condensation of 5-(diethylamino) salicylaldehyde and hydrazine with pyrrole-2-carbaldehyde. Their structures were confirmed based on CHN, UV−visible, FT-IR, and EPR measurements. The complexes were also assessed for their antibacterial, antioxidant, and anticancer properties. Some of these chemicals were said to be extraordinarily effective in this respect. The antibacterial activities of the complexes in vitro demonstrated their potential, although the [Cu(L)(bpy] complex was suggested to exhibit moderate activity against pathogens compared to all other in this series. The cytotoxic activity of the prepared analogues showed better cell viability compared with standard cisplatin. Moreover, there is a good agreement between the experimental and theoretical findings from docking and theoretical investigations done using DFT at the B3LYP level.

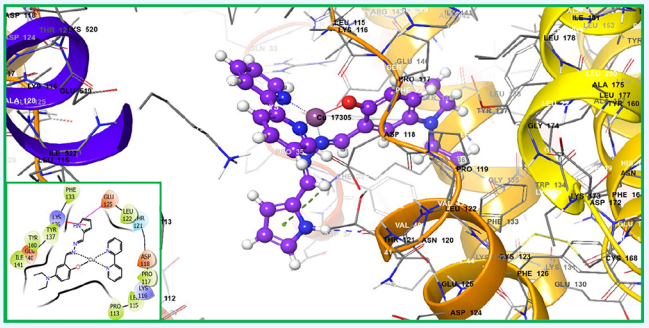

1. INTRODUCTION

Transition metal complexes made from Schiff bases have drawn attention of scientists for their versatile transformations via reductions, condensations, and additions, respectively. These transformations have led to the synthesis of major pharmacological and biochemical compounds.[1,2] According to recent investigations, these complexes also exhibit antimicrobial, photocatalytic, and chemotherapeutic properties and could be employed as mimic systems for enzyme models.[3−5] Only a few of the synthesis techniques have been described thus far, including the coupling of alcohols and amines, dimerization, oxidation, or dehydrogenation of primary amines, and others.[6,7] Due to the widespread availability of starting amines, the most common and efficient imines has traditionally been made by the condensation of active aldehydes and amines.[8]

One of the most notable simple heterocycles found in marine natural products, including dimeric compounds like nakamuric acid, is the pyrrole.[9] Due to their synthesis and biological activity, coordination complexes containing pyrrole and its derivatives have drawn a lot of attention.[10,11] Azines are a well-known family of chemical compounds, with intriguing characteristics and widespread applications in dyes.[12] The azine moiety is widely found in both natural products and bioactive chemicals. As a result, organic chemistry has given a lot of thought to the creation of efficient methods for creating these frameworks. The fields of medical chemistry and biochemistry might gain from such a synthetic campaign by using these coupled heterocycles as lead compounds in drug development. Open-chain diazine Schiff base ligands are of tremendous interest since they could give birth to a large variety of coordination compounds with different binding modes due to their rotational flexibility around the N−N bond and possible donor sites.[12] Numerous studies have been conducted on metal complexes including salicylaldehyde and its derivatives as Schiff base ligands. Such ligands are rather frequent in metal complexes, which also demonstrate their simplicity, adaptability to various structural alterations, and broad applications in areas including catalysis, biological systems, and material chemistry.[13−16]

As a result, our approach was to synthesize novel donor site-added pyrrole-based Schiff base ligands. The Schiff base ligands were synthesized via the condensation of (E)-2-(hydraziney-

Received: April 26, 2023
Accepted: August 10, 2023
Published: September 14, 2023

lidenemethyl)-1H-pyrrole with 5-(diethylamino)-2-hydroxybenzaldehyde. A novel set of nickel(II), copper(II), and zinc(II) complexes were created in order to use the ligands. Using the MTT assay, the complexes' in vitro anticancer activity was evaluated against the colon cells (HCT116), cervical epidermoid carcinoma cells (CaSki), and breast cancer cells (MCF7). The antibacterial effect and free radical scavenging ability were investigated by a disc diffusion assay and a DPPH radical scavenging assay, respectively. According to DFT, the frontier molecular orbital for all metal(II) complexes was analyzed by using the B3LYP/LACVP++ function. Additionally, to determine the complexes' affinities for the bovine receptor, molecular docking studies were conducted.

2. EXPERIMENTAL PART

2.1. Materials and Methods. The compounds used for the synthesis of the ligand include 5-(diethylamino) salicylaldehyde, pyrrole-2-carbaldehyde, and hydrazine, which were obtained from Alfa Aesar. An AR-grade 2,2′-bipyridyl and hydrated metal salts like manganese(II) chloride tetrahydrate, nickel(II) chloride hexahydrate, copper(II) chloride dehydrate, and zinc(II) chloride were obtained from Sisco Research Laboratories. For spectroscopic analysis, the HPLC-grade solvents, dimethyl formamide (DMF) and dimethyl sulfoxide (DMSO), were purified before use. The C, H, and N contents of complexes were analyzed using a Carlo Erba Elemental analyzer Model 1106. An infrared spectrum was recorded on the Perkin-Elmer FT-IR (ATR mode) type spectrophotometer in the range between 4000 and 400- cm-1. UV spectra were analyzed in HPLC-grade ethanol on a Perkin-Elmer Lambda-35 spectrophotometer operating in the range of 200−900 nm. The electrospray mass spectra of complexes were recorded in positive mode on the Q-Tof-Mass spectrometer. Electron paramagnetic resonance (EPR) spectra were recorded on the JES-X310 X-band EPR spectrometer at room temperature.

2.2. Cell Culture. The MCF7, CaSki, and HCT116 cancer cell lines were provided by the National Centre for Cell Sciences (NCCS), Pune, India, and nutrient medium including DMEM was given access by Gibco, Invitrogen. The cells were cultured in a 25 cm_2 tissue culture flask with DMEM supplemented with 10% FBS, L-glutamine, and sodium bicarbonate as well as the antibiotic solution containing penicillin (100 U/mL), streptomycin (100 g/mL), and amphotericin B (2.5 g/mL). Cultured cell lines were kept at 37 °C in a humidified 5% CO_2 atmosphere.

2.3. Synthesis of the Ligand (HL). The Schiff base ligand, 2-((E)-(((E)-(1H-pyrrol-2-yl)methylene)hydrazineylidene)-methyl)phenol [**HL**], was synthesized by the following procedure: an ethanol solution (30 mL) of 5-(diethylamino)-2-hydroxybenzaldehyde (5 mmol) was gradually added to an ethanol solution (30 mL) of (E)-2-(hydrazineylidenemethyl)-1H-pyrrole (5 mmol) with constant stirring in the presence of acetic acid (3 drops) as a catalyst. The acquired product was dried in a vacuum desiccator and crystallized with dry ethanol. Yield: (76%). Color: pale brown. M.p.130 °C. Anal. calcd for $C_{16}H_{20}N_4O$. Found (calcd) (%): C, 67.34 (67.58); H, 6.89 (7.09); N, 19.61 (19.70); ^{1}H NMR ($CDCl_3$, Δ, PPM) 10.5(Ar−OH), 8.32 (N═CH), 6.1−7.59 (Ar-ring), C^{13} NMR ($CDCl_3$ Δ, PPM) 154.39 (Ar−C−OH), 152.59 (N═CH).IR (ν, cm^{-1}): 3280 (ν −OH); 1682 (ν C═N); (λ_{max}/nm) in MeOH: 262 ($\pi-\pi^*$), 353 (180), 351 ($n-\pi^*$). ESI-MS (m/z): 293.14.

2.4. Synthesis of Metal(II) Complexes. *2.4.1. [M^{1-4}(L)].* The manganese(II) **1**, nickel(II) **2**, copper(II) **3**, and zinc(II) **4** complexes were prepared by the following procedure: An ethanolic solution (30 mL) of $NiCl_2$ (0.29 g, 1.2 mmol), $CuCl_2$ (0.29 g, 1.2 mmol), $ZnCl_2$ (0.36 g, 1.2 mmol), and $MnCl_2$ (0.36 g, 1.2 mmol) was added to an equimolar solution of ligand (HL, 1.2 mmol) in ethanol (30 mL) and then stirred at a constant speed. The crude sample was recrystallized from hot ethanol and dried in vacuum over P_4O_{10}.

2.4.2. [M^{5-8}(L)(Bpy)]. To an ethanolic solution, an equimolar (1:1:1) mixture of **HL** (2 mmol), metal(II) salts (2 mmol), and 2,2′ bipyridyl (2 mmol) was added and refluxed with stirring for about 8 h to get the corresponding product of manganese(II) (**5**), nickel(II) (**6**), copper(II) (**7**), and zinc(II) (**8**) complexes.

2.5. In Vitro Antibacterial Assay. The synthesized compounds' effectiveness against four bacterial strains was assessed, including *Enterococcus faecalis* ATCC, methicillin-resistant *Staphylococcus aureus* (MRSA) ATCC33591, *Klebsiella pneumoniae* ATCCBAA-1705, and *Acinetobacter baumannii* ATCC19606. The antimicrobial activity was investigated by disc diffusion assay, determining the minimum inhibitory concentrations (MICs). In order to check whether the synthesized complex has any antimicrobial efficacy against bacteria, the compound was assayed on a petri dish containing Mueller-Hinton agar to determine the antibacterial activity against each bacteria. The assay was performed by Kirby-Bauer antibiotic susceptibility test.[17] Briefly, an overnight culture of each bacterial strain was grown to the mid-logarithmic phase at 37 °C in a shaking incubator. The synthesized complex compound was dissolved in methanol or DMSO, loaded as a 50 μL volume containing 25 μg of compound on the sterile 6 mm diameter disc (HiMedia), and allowed to dry. Bacterial culture was swabbed on the Mueller-Hinton agar plate, and discs were placed on the plates, incubated at 37 ° C for 24 h, and observed for the presence of an inhibition zone. The compound showing antibacterial activity was further used for MIC assay.

The MIC of compounds was evaluated using the broth microdilution method.[18] The synthesized metal complex compounds were dissolved in dimethylsulfoxide (DMSO, Fisher Chemicals) as a stock solution and serially diluted in Mueller-Hinton Broth (MHB) for bacteria to obtain a concentration range of 512 to 0.25 μg/mL. Then, 10 μL of each concentration was added into a 96-well microplate well containing 90 μL of MHB and 10 μL of 1×10^5 CFU/mL of bacterial inoculum to acquire a final concentration range of 256 to 0.125 μg/mL. The inoculated microplates were covered and incubated at 37 ° C for 24 h. MICs were assessed at which no bacterial growth was assessed. Ciprofloxacin (12 μg/mL) was used as the positive control, and the negative control was added with DMSO.

2.6. In Vitro Cytotoxicity Analysis. An inverted phase-contrast microscope was used to directly observe the cells in order to assess their qualitative viability. Cellular viability was evaluated quantitatively using the MTT test. Trypsinized 48 h old confluent monolayers of cells were seeded in 96-well tissue culture plates at a density of 5×10^4 cells/well, suspended in a 10% growth medium, and kept at 37 °C in a humidified 5% CO_2 incubator. Using a cyclomixer, 1 milligram of a metal complex sample was measured and dissolved in 1 mL of DMSO. To assure sterility, the sample solution was passed through a 0.22-m Millipore syringe filter. Following a 24-hour

https://doi.org/10.1021/acsomega.3c02860
ACS Omega 2023, 8, 34458−34470

incubation period, the growth medium was discarded, and 5 times serial dilutions of freshly produced compounds in 5% DMEM were carried out. Then, three replicates of each concentration of 100 L were added to the appropriate wells. After that, the mixture was incubated at 37 °C in a humidified 5% CO_2 incubator.

The entire plate was observed after 24 h of treatment in an inverted phase-contrast tissue culture microscope (Olympus CKX41 with an Optika Pro5 CCD camera), and microscopic observations were recorded as images. Any noticeable changes in the morphology of the cells, for instance, rounding or shrinking of cells, granulation, and vacuolization in the cytoplasm of the cells were considered a sign of cytotoxicity.

After 24 h of the incubation period, the sample content in the wells was removed, and 30 μL of reconstituted MTT solution was added to all test and cell control wells. The plate was gently shaken well and then incubated at 37 °C in a humidified 5% CO_2 incubator for 4 h. 15 mg of MTT (Sigma, M-5655) was reconstituted in 3 mL of PBS until completely dissolved and sterilized by filter sterilization. After the incubation period, the supernatant was removed, and 100 μL of MTT solution was added. The absorbance values were measured by using a microplate reader at a wavelength of 540 nm.

The percentage of growth inhibition was calculated using the formula:

Mean OD of control group

$$\%\text{of viability} = \text{mean OD samples} \times 100$$

2.7. Antioxidant Assay. Free radical scavenging ability of the synthesized compounds was tested by DPPH assay as described by Munira et al.[19] In the presence of antioxidants, DPPH normally turns a methanol solution violet or purple and fades to yellowish tones. 2.4 mL of a 0.1 mM (DPPH) solution in methanol was mixed with 1.6 mL of the test ligand in methanol at varied concentrations (10−100 g/mL). The reaction mixture was held at RT for 30 min in the dark after it had fully vortexed. The absorbance of the combination was measured spectrophotometrically at 517 nm. BHT (butylated hydroxytoluene) was used as a reference. The percentage DPPH radical scavenging activity was calculated by the following equation:

$$\%\text{DPPH radical scavenging activity} = \{(A_0 - A_1)/A_0\}2 \times 100$$

where A_0 is the absorbance of the control and A_1 is the absorbance of the extractives/standard. Then, % of inhibition was plotted against concentration, and from the graph, IC_{50} was calculated.

2.8. Computational Study. The computational program was carried out using jaguar v9 program, which is incorporated in Schrödinger suite 2018.[20] Metal complexes were optimized over density functional theory (DFT) using the B3LYP functional, and the LACVP++ basis set was used in all cases.

2.8.1. Frontier Molecular Orbital Analysis (FMO's). In complexes, a FMO analysis primarily studies the electron transition of a compound between the highest occupied molecular orbitals (HOMO) and the lowest unoccupied molecular orbitals (LUMO), while the former acts as electron-donating species or nucleophiles and the latter as electron-accepting species or electrophiles in nature.[21] The calculated energy values of HOMO and LUMO provide more information about the complexes.

2.8.2. Molecular Docking Studies. Rigid molecular docking studies have been carried out by the glide docking program (maestro 11.2v) provided by the Schrodinger suite 2015−2 modeling package installed on an Intel Pentium 32 bit; x64 processor-based HP workstation with a Windows-10 operating system.[22] The molecular docking study was accomplished with the aim of observing binding sites on BSA and binding affinity of the protein-ligand complex. The 3D structure of all the complexes was built in a maestro builder panel. In the ligand preparation wizard, the 3D structure of complexes is executed to add hydrogen atoms and regulate rational bond angles, geometry, and ring conformations. Then, the complexes were optimized by using force field potentials for liquid simulations (OPLS-2005), and thereafter, minimization was done until it reached a 0.01 Å root mean square deviation (RMSD).[23] The subsequent output structures of complexes were suitable for docking with the BSA receptor.

The crystal structure of BSA (PDB: 3V03) was obtained from the website (http://www.rcsb.org). All the pre-ligands and H_2O molecules in the receptor were removed. Then, it was fully optimized in the protein preparation wizard (adding polar hydrogen atoms, bond order, and protonation states and deleting water beyond 5 Å), minimizing the structure by using the force field OPLS-2005. The minimized BSA receptor was fit for docking with prepared complexes. The preparation of the grid file was done by supplying *x*, *y*, and *z* coordinates of −8.857, 61.031, and 14.77 Å, respectively, and with a grid box diameter (*xyz*) of 30 × 30 × 30 Å with a grid resolution of 0.3 Å. The 3D and 2D interactions were visualized in maestro workspace.

2.8.3. Geometry Optimization. Geometry optimization is a technique to predict the 3D arrangement of the atoms in a molecule and provide information regarding geometry via minimization of energy. It involves a sequence of iterations accomplished until the energy of the molecule has attained a minimum. At the end of optimization, the molecules attained a new geometry and energy. By this way, the geometry optimization for synthesized metal(II) complexes **1**−**8** was carried out based on density functional theory using function B3LYP and basis set LACVP++.[9] The LACVP++ was the effective core basis set because it is a combination of the 6-31G basis set with LANL2DZ. The optimized molecular structure of the metal(II) complexes is illustrated in Figure S2, and the selected bond angles and bond lengths are given in Tables S1 and S2. The resulting bond angles and bond lengths were found to be more appropriate to predict the geometry of the metal(II) complexes. For four coordinate systems, the molecular structure of the complexes was decided by the geometric parameter "τ", and it is calculated by using the formula.[10]

$$\tau \approx -0.00709\alpha - 0.00709\beta + 2.55$$

β = axial bond angle

α = equatorial bond angle

When τ is close to 0, the geometry is similar to square planar, while if τ close to 1, it is tetrahedral geometry. In our complexes **1**−**4,** the calculated τ values were 0.94, 0.78, 0.67, and 0.82, respectively, which suggested tetrahedral geometry due to τ values that lie near 1, while for the complexes **5**−**8,**

https://doi.org/10.1021/acsomega.3c02860
ACS Omega 2023, 8, 34458−34470

the calculated τ values were 0.24, 0.22, 0.20 and 0.26, suggesting square planar geometry due to τ values near zero.

3. RESULTS AND DISCUSSION

In this series, metal complexes of the type [M(L)] (**1**−**4**) were prepared by reacting an equimolar mixture of the Schiff base

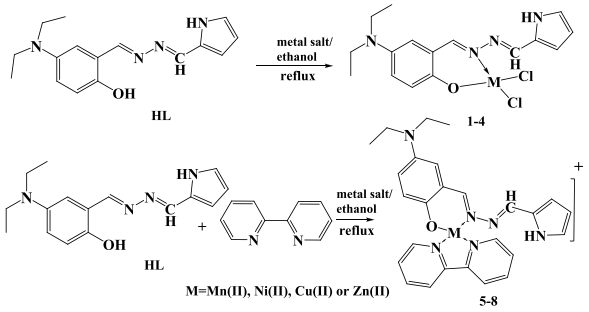

Figure 1. Synthesis of complexes of type [M(L)] (**1**−**4**) and [M(L)(bpy)] (**5**−**8**).

ligand (**HL**) and metal salts. Likewise, [M(L)(bpy)] (**5**−**8**) type complexes were synthesized using the 1:1:1 stoichiometric mixture of **HL**, 2,2′-bipyridyl, and metal(II) salts under methanolic conditions as shown in Figure 1. All the complexes were obtained in good yield and were soluble in organic solvents such as acetonitrile, DMSO, methanol, and DMF. The physical and analytical results of the complexes are displayed in Table 1.

The FT-IR spectrometric method was used to obtain the IR spectrum of the synthesized complexes in the 400−4000 cm^{-1} range in ethanol.[24−26] The peak annotations of the present complexes are summarized in Table 2. The O-H stretching band was not detected at 3350 cm^{-1}, which proposes that phenolic O−H is deprotonated because of complex generation. The absence of carbonyl stretching ν(C═O) and, simultaneously, the existence of azomethine stretching at 1650 to 1690 cm^{-1} confirm the −C═N coordination toward metal ions.[18,19] The peaks observed in the region 1450−1480 cm^{-1} confirmed the presence of different delocalized ligand moieties 2,2′-bipyridyl coordinated to the metal ions through imine nitrogen ν(C═N). The weak intense bands are located in the region around 480−505 cm^{-1} and 545−570 cm^{-1} assigned to ν(M−N) and ν(M−O), respectively, in both [M(L)] (**1**−**4**) and [M(L)(bpy)] (**5**−**8**) type complexes, and this substantiates coordination of the ligand to metal ions.[27]

^{1}H NMR spectra were recorded in $CDCl_3$ using tetramethylsilane as an internal standard and are provided in the Supporting Information. The ^{1}H NMR spectrum of the zinc complex 8 is depicted also in Figure S1.The Schiff base of the complex exhibited a sharp singlet in 8.32 ppm, attributing to the azomethine (−CH═N−) proton which undergoes downfield shifting at 9.20 ppm in the case of the Zn(II) complex of the Schiff base. A hydroxyl proton singlet for the ligands was observed in the range 10.5 ppm that is absent in the spectra of complexes, indicating deprotonation and organization of the oxygen anion with the central metal ion. The ^{1}H NMR spectrum results evidently suggests the ligation behavior of Schiff's base in a bidentate manner and confirms the proposed structure of the metal complexes as shown in Figure S2. The C^{13} NMR spectrum of zinc complex 8 is depicted also in Figure S1. The Schiff base of the complex exhibits a singlet in 155.17 ppm, attributing to azomethine carbon (−CH═N−) (Figure S3).

The absorption spectra of complexes (**1**−**8**) were recorded using ethanol at 298 K (Figure 2), and their annotations are summarized in Table 2. The strong band at 220−300 nm is due to intra-ligand charge transfer transition (π−π* and n−π*). The medium band at 330−390 nm was appropriate for ligand to metal charge transfer transition (LMCT).[28] The d-d transition band for Cu(II) and Ni(II) complexes displayed one weak absorption bands around 630−705 nm, suggesting square planer geometry around the metal ion.[11] As spin is forbidden, the manganese complexes do not reveal any peaks in the d-d region. However, Zn(II) complexes (**4**) and (**8**) did not show any kind of peak in the visible spectra caused by diamagnetic and d^{10} electronic configuration.[29]

The electrospray ionization (ESI) mass measurements of complexes (**1**−**8**) were recorded in positive mode, which is consistent with the suggested molecular structure of metal(II) complexes. For example, the complex [Mn(L)] (**1**) (Figure 3a) exhibited a ionic peak at m/z = 409.27, which corresponds to the $[C_{16}H_{19}Cl_2MnN_4O]^+$fragment. Moreover, the spectrum exhibits other fragment peaks at m/z = 338.22 and 266.02, corresponding to $[C_{16}H_{19}MnN_4O]^+$ and $[C_{12}H_9C_{l2}MnN_3O]^+$ respectively. The mixed ligand stoichiometric metal(II) complex for [Mn(L)(bpy)] (**5**) (Figure 3b) showed peaks at m/z = 494.3 and 338.2 for a molecular ion peak and base peak, respectively, which correspond to $[C_{26}H_{27}MnN_6O]^+$ and $[C_{16}H_{19}MnN_4O]^+$.

The solid state ESR spectra of complexes [Cu(L)](**3**)and-[Cu(L)(bpy)](**7**) (Figure 4a,b) were recorded in DMF at 298 K, and their "g" tensor values confirm that the complexes exhibit axial symmetry. The ground state of copper(II) complex unpaired electron lies in the $d_{x^2-y^2}$ molecular orbital, having $^2B_{1(g)}$ as the ground state with $g_{\|} > g_{\perp} > 2.0023$.[26] The spin Hamiltonian parameters of the Cu(II) complex at $g_{\perp}$ and $g_{\|}$ have the values 2.073 and 2.147, 2.178, and 2.25,

Table 1. Physical and Analytical Data of Metal(II) Complexes (1−8)

						found (calcd) (%)		
complexes	f	color	m. wt. (g/mol)	m.p. (°C)	yield (%)	C	H	N
[**Mn(L)**] (**1**)	$C_{16}H_{19}Cl_2MnN_4O$	brown solid	409.27	<250	78	46.91 (46.96)	4.70 (4.68)	13.71 (13.60)
[**Ni(L)**] (**2**)	$C_{12}H_{10}Cl_2N_3NiO$	pale green	413.02	<250	80	46.44 (46.54)	4.58 (4.64)	13.49 (13.57)
[**Cu(L)**] (**3**)	$C_{16}H_{19}Cl_2CuN_4O$	brown solid	418.02	<250	83	46.32 (46.00)	4.52 (4.58)	13.38 (13.41)
[**Zn(L)**] (**4**)	$C_{16}H_{19}Cl_2N_4OZn$	pale yellow	419.02	<250	73	45.2 (45.2)	4.52 (4.56)	13.25 (13.35)
[**Mn(L)(bpy)**] (**5**)	$C_{26}H_{27}MnN_6O$	brown solid	494.3	<250	77	62.94 (62.68)	4.98 (5.46)	16.92 (16.87)
[**Ni(L)(bpy)**] (**6**)	$C_{26}H_{27}N_6NiO$	pale green	498.16	<250	84	62.62 (51.51)	5.5 (3.93)	16.91 (8.19)
[**Cu(L)(bpy)**] (**7**)	$C_{26}H_{27}CuN_6O$	brown solid	503.16	<250	82	61.87 (62.07)	5.21 (5.41)	16.61 (16.71)
[**Zn(L)(bpy)**] (**8**)	$C_{26}H_{27}N_6OZn$	pale yellow	507.15	<250	75	61.65 (61.85)	5.27 (5.39)	16.54 (16.64)

https://doi.org/10.1021/acsomega.3c02860
ACS Omega 2023, 8, 34458−34470

Table 2. FT-IR and UV−Visible Spectral Data of Metal(II) Complexes (1−8)

	FT-IR spectral data (cm^{-1})				UV−visible spectral data (λ_{max}/nm)
complexes	ν(−C═N−)	ν(M−O)	ν(M−N)	d−d	charge transfer
HL	1682				351($n-\pi^*$), 262($\pi-\pi^*$)
[Mn(L)] (1)	1663	545	480		226 ($\pi-\pi^*$), 267 ($n-\pi^*$), 337 (LMCT)
[Ni(L)] (2)	1658	556	482	678	253 ($\pi-\pi^*$), 287 ($n-\pi^*$), 387 (LMCT)
[Cu(L)] (3)	1656	552	490	701	258 ($\pi-\pi^*$), 282 ($n-\pi^*$), 371 (LMCT)
[Zn(L)] (4)	1650	558	495		271 ($\pi-\pi^*$), 293 ($n-\pi^*$), 375 (LMCT
[Mn(L)(bpy)] (5)	1652	550	498		251 ($\pi-\pi^*$), 303 ($n-\pi^*$), 387 (LMCT)
[Ni(L)(bpy)] (6)	1663	549	500	630	236 ($\pi-\pi^*$), 296 ($n-\pi^*$), 378 (LMCT)
[Cu(L)(bpy)] (7)	1664	557	501	653	240 ($\pi-\pi^*$), 300 ($n-\pi^*$), 376 (LMCT
[Zn(L)(bpy)] (8)	1659	566	495		273 ($\pi-\pi^*$), 295 ($n-\pi^*$), 374 (LMCT)

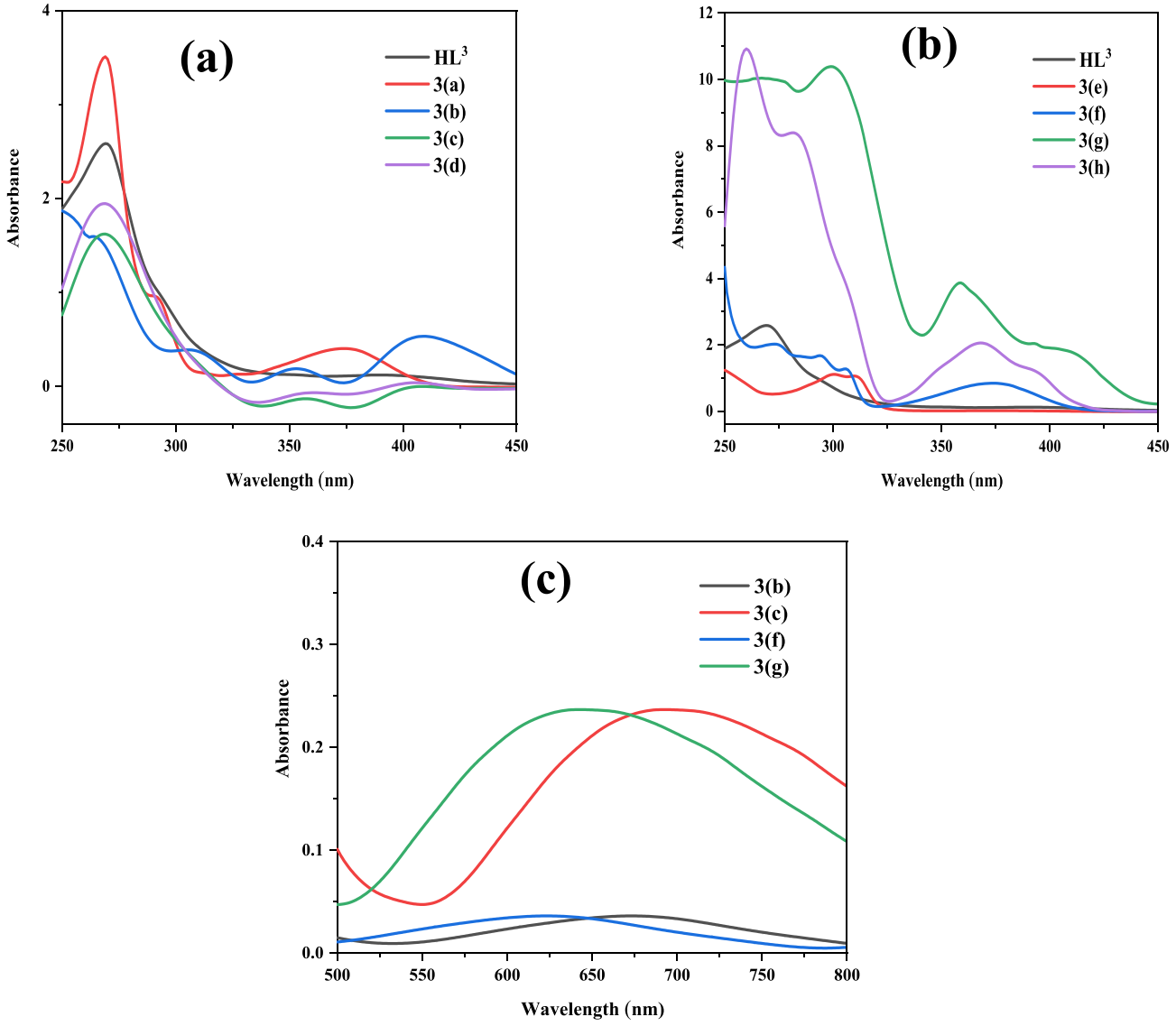

Figure 2. UV spectra of (a) complexes (1−4), (b) complexes (5−8), and (c) visible spectra of complexes (2), (3), (6), and (7) in methanol.

respectively. However, the complex[Cu(L)(bpy)](7) showed $g_{\parallel}$ = 2.148, 2.178 and 2.244, $g_{\perp}$ = 2.054, suggesting the complex to have square-planar geometry. In addition to axial symmetry, the "g" tensor values are related by formula $G = (g_{\parallel} - 2) / (g_{\perp} - 2)$, where G relates the exchange interaction parameter according to Hathway and billing.[30] If $G > 4.0$, the exchange interaction between the Cu(II) center in the crystalline state is a negligibly considerable interaction occurring in a complex, whereas when it is $G < 4.0$, considerable interaction was taking place. The calculated G values for complexes (3) and (7) were 4.6 and 4.38, respectively, which were reliable with a $d_{x^2-y^2}$ ground state in a square planar geometry[31] and suggested that no exchange interaction takes place in the polycrystalline state.

The XRD spectra of the complexes (1−8) are exhibited in Figures 5 and 6. The high intense diffraction peaks observed for Mn(II) (1) and (5), Ni(II) (2) and (6), and Cu(II) (3) &

https://doi.org/10.1021/acsomega.3c02860
ACS Omega 2023, 8, 34458−34470

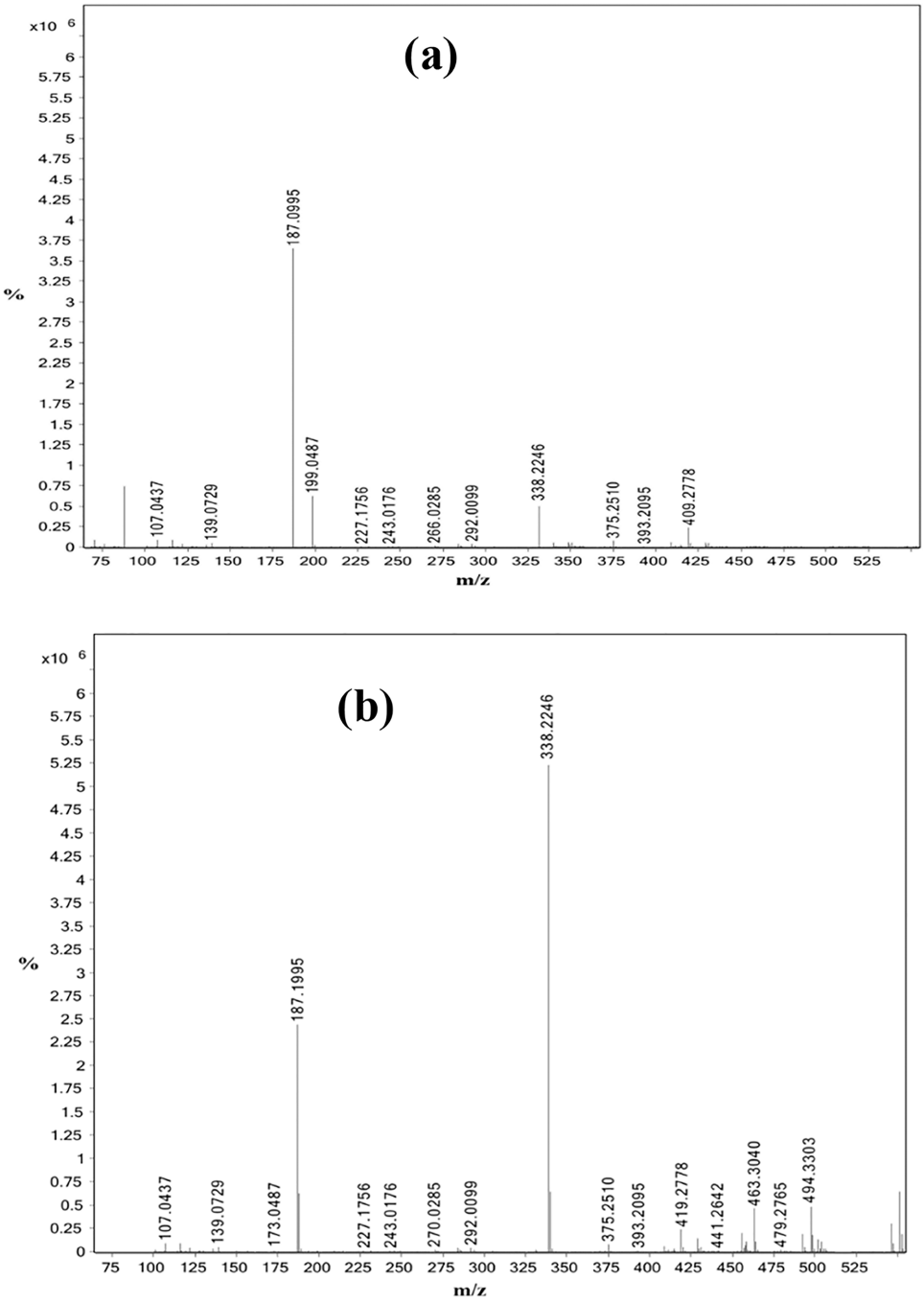

Figure 3. ESI mass spectrum of (a) [Mn(L)] (**1**) and (b) [Mn(L)(bpy)] complex (**5**) in methanol.

(7) complexes at around 5−60° indicate that complexes have a fine polycrystalline phase, whereas Zn(II) (**4**) and (**8**) complexes showed only few reflection peaks, suggesting the existence of both crystalline and amorphous nature.[15] The average crystallite size of the complex was calculated from Scherre's formula.[32−34] From the calculated data, the average crystallite size of samples was found to be in the range of 40−70 nm.

The TGA curve of complex [Cu(L)(bpy)] (**7**) shows four consecutive steps of degradation within the range of 38−800 °C (Figure 7). It is clear that the weight loss of M(II) complexes correlates with comparing different compositions at a specific temperature. The first decomposition temperature arises between 50 and 110 °C and corresponds to the loss of one molecule of lattice water with a mass loss of 3.14% (calcd 3.42%). After dehydration, degradation of the dehydrated complex molecule occurs at the next consecutive stages due to the loss of its organic backbone. The second and third stage involves a loss of the organic moiety HL ligand fragment at a temperature range of 110−305 °C, corresponding to the mass loss 34%. Then, at the fourth step (305−710 °C), there is a mass loss of the pyrrole moiety in the metal complexes. No further mass loss is seen from 710 °C to around 800 °C because of CuO formation, which indicates good thermal stability of the complex. A similar behavior was detected in the TGA plots of other complexes.

The FMO analysis represented in the highest occupied molecular orbital (HOMO) and lowest unoccupied molecular

https://doi.org/10.1021/acsomega.3c02860
ACS Omega 2023, 8, 34458−34470

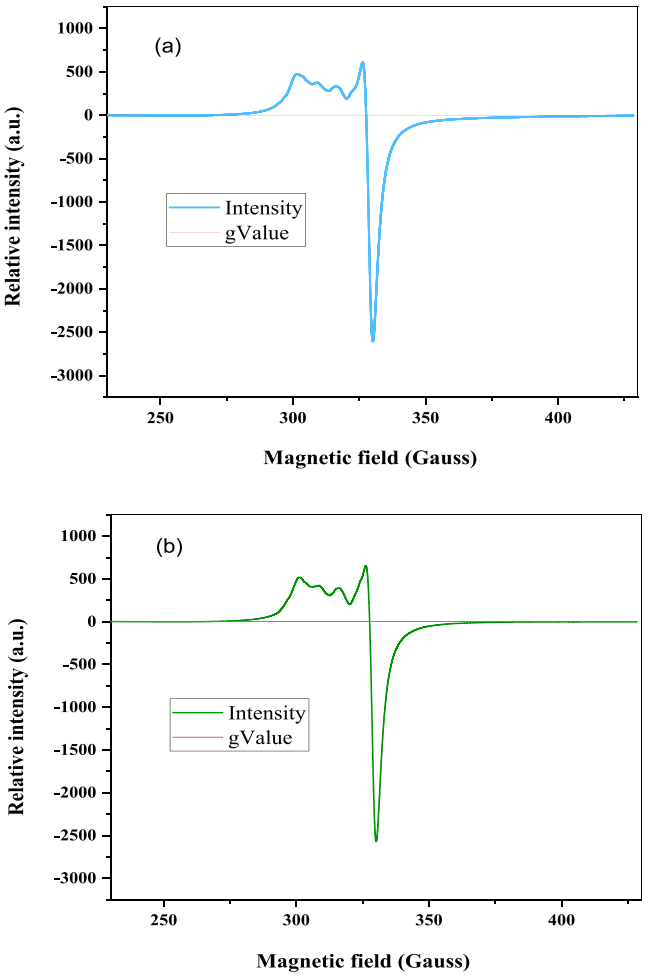

Figure 4. X-band EPR spectrum of complex (a) [Cu(L)] (**3**) and (b) [Cu(L)(bpy)] (**7**) at room temperature.

orbital (LUMO) plays an important role in determining chemical activities of the molecule as well as optical and electric properties. This method clearly pictured the energies of the HOMO and LUMO.[15] The energy differences (ΔE) of HOMO−LUMO were considered an important parameter for enlightening the structure and reactivity. The molecular orbitals of complexes are illustrated in Figures 8 and 9. According to Koopman's approximation theorem, some other important quantum parameters such as the HOMO−LUMO bandgap (ΔE), chemical potentials (Pi), absolute electronegativities (χ), absolute softness (σ), absolute hardness (η), global electrophilicity (ω), global softness (S), and additional electronic charge (ΔN_{max}) were evaluated using the described equations in ref 35.

The band gap is an important parameter to determine the activity or stability of compounds. A molecule with low ΔE values is associated with more polarizability and high reactivity, has low kinetic stability, and is termed the soft molecule. In this study, the calculated quantum parameters, such as ΔE, η, χ, σ, S, Pi, ω, and ΔN_{max}, are shown in Table 3. The-E_{HOMO} values were − 5.353, −5.884, −5.584, −5.645, −3.721, −4.034, −2.710, and −3.915 eV, while E_{LUMO}-values were − 2.750, −4.098, −4.244, −2.412, −1.500, −1.913, −1.598, and −1.905 eV, corresponding to metal(II) complexes (**1**−**8**). The differences of HOMO−LUMO (ΔE) for complexes (**1**−**8**) were found to be 2.60, 1.79, 1.34, 3.23, 2.22, 2.12, 1.11, and

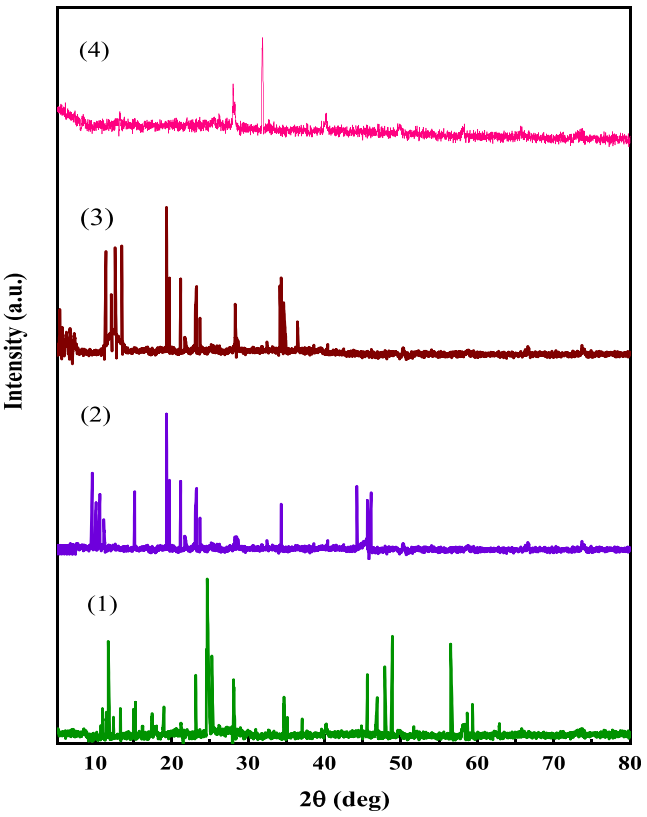

Figure 5. Powdered X-ray patterns of complexes (**1**−**4**).

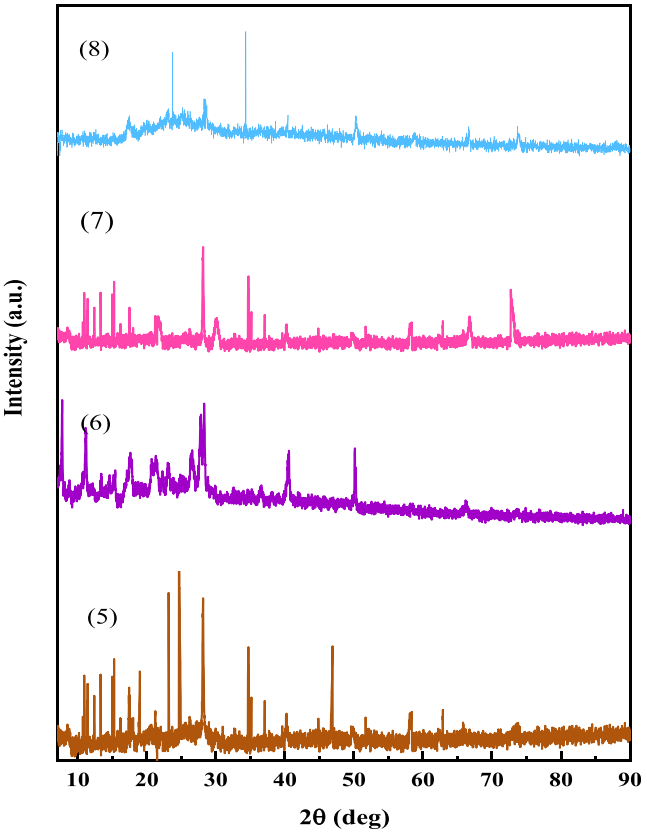

Figure 6. Powdered X-ray patterns of complexes (**5**−**8**).

2.01 eV respectively. The negative convention for the HOMO−LUMO due to the zero point on the energy scale

https://doi.org/10.1021/acsomega.3c02860
ACS Omega 2023, 8, 34458−34470

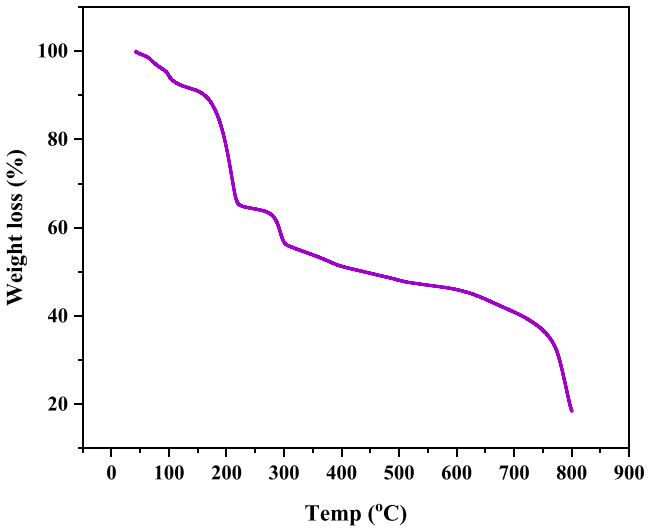

Figure 7. TGA curve of complex [Cu(L)(bpy)] (**7**).

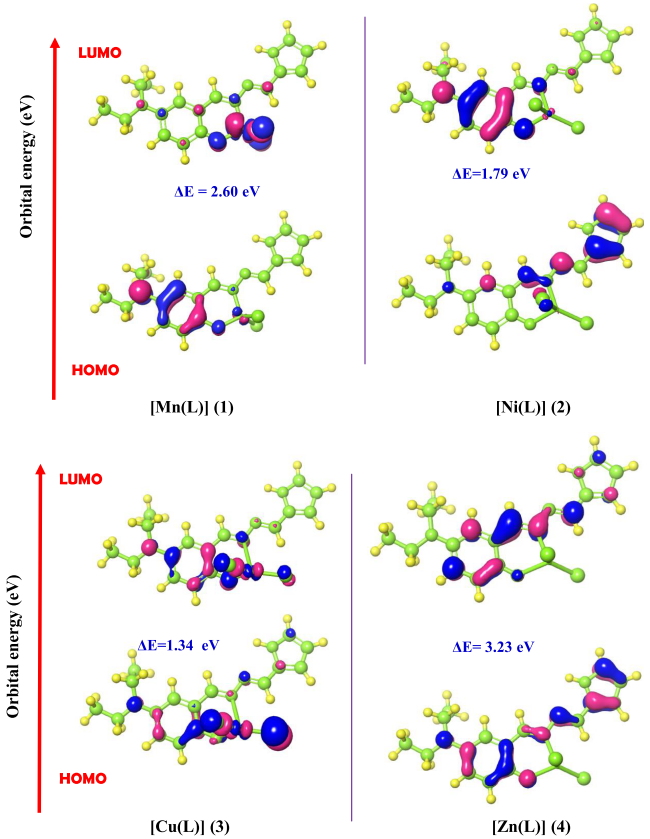

Figure 8. Frontier molecular orbital of investigated complexes [Mn(L)] (**1**), [Ni(L)] (**2**), [Cu(L)] (**3**), and [Zn(L)] (**4**) using the B3LYP/LACVP++ basis set.

corresponds to an infinite separation of the electron from the molecule, so any electron in an orbital (HOMO or LUMO, bonding or antibonding) corresponds to a more stable state than an infinite separation and therefore would have a negative energy. It was observed that the mixed ligand Cu(II) complex (**7**) exhibited the least bandgap. The lesser band gap preferred easy transitions of electrons from the ground state to the excited state. Moreover, the biological activity of complexes is influenced by the smaller bandgap.

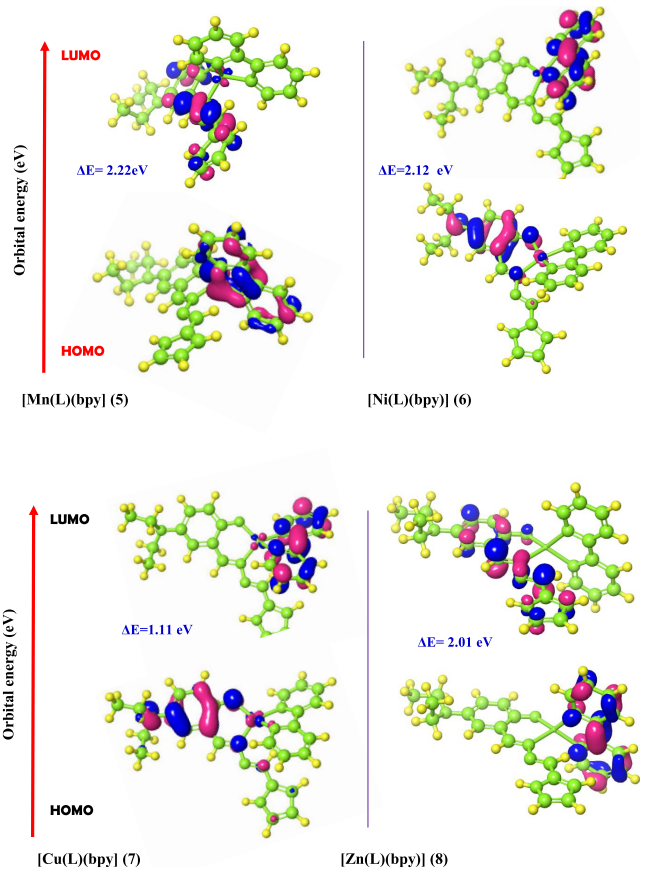

Figure 9. Frontier molecular orbital of investigated complexes [Mn(L)(bpy)] (**5**), [Ni(L) (bpy)] (**6**), [Cu(L) (bpy)] (**7**), and [Zn(L) (bpy)] (**8**) using the B3LYP/LACVP++ basis set.

A theoretical approach for checking the bioactivities of the synthesized metal(II) complexes was done by molecular modeling computation. Here, the prepared complex was docked into the preferred site on the crystal structure of protein BSA (PDB ID: 3V03), which is downloaded from the protein data bank. The metal(II) complexes and the target protein BSA were optimized by using force field OPLS-2005.[36] All docked metal complexes are represented as a ball and stick model; to clarify, the preferred docking score of complexes in the target protein is shown in Table 4. From the figure, it is clear that the active sites of the docked protein is well stabilized by the H-bond, $\pi-\pi$ stacking interactions, and numerous hydrophobic contacts. The observed docking score values of complexes (**1**−**4**) with the BSA receptor are −5.836, −6.374, −5.824 and −5.711 kcal/mol, respectively. The 3D images of complexes showed H-bond interaction with LYS 116 and numerous hydrophobic contacts. Similarly, mixed ligand type complexes (**5**−**8**) show −5.382, −5.643, −6.856, and −5.471 kcal/mol. The 3D images of these type complexes revealed H-bond interaction with residue LYS 136 and GLU 140. Cu(II) (**7**) (Figure 10) showed the highest docking score compared to others, and it was influenced by bipyridyl ligand stronger covalent coordination with copper metal ions than the others. The more binding affinity of this complex is due to the hydrogen bond, pi−pi stacking, and large number of hydrophobic contacts with the receptor. From this, we can say that, in this series, complex (**7**) is more potent against the BSA receptor.

https://doi.org/10.1021/acsomega.3c02860
ACS Omega 2023, 8, 34458−34470

Table 3. Calculated Quantum Parameters of the Metal(II) Complexes (1−8)

complexes	HOMO (eV)	LUMO (eV)	ΔE (eV)	χ	η	σ	Pi	S	ω	ΔN_{max}
[Mn(L)] (1)	−5.353	−2.750	2.60	4.05	1.30	0.77	−4.05	0.65	10.7	3.11
[Ni(L)] (2)	−5.884	−4.098	1.79	4.99	0.89	1.12	−4.99	0.45	11.1	5.59
[Cu(L)] (3)	−5.584	−4.244	1.34	4.91	0.67	1.49	−4.91	0.34	8.1	7.33
[Zn(L)] (4)	−5.645	−2.412	3.23	4.03	1.62	0.62	−4.03	0.81	13.1	2.49
[Mn(L)(bpy)] (5)	−3.721	−1.500	2.22	2.61	1.11	0.90	−2.61	0.56	3.8	2.35
[Ni(L)(bpy)] (6)	−4.034	−1.913	2.12	2.97	1.06	0.94	−2.97	0.53	4.7	2.80
[Cu(L)(bpy)] (7)	−2.710	−1.598	1.11	2.15	0.56	1.80	−2.15	0.28	1.3	3.87
[Zn(L)(bpy)] (8)	−3.915	−1.905	2.01	2.91	1.01	0.99	−2.91	0.50	4.3	2.90

Table 4. Molecular Docking Parameters of the Metal(II) Complexes (1−8) with the BSA Receptor

		active sites with a mode of interaction		
complexes	docking score, kcal mol^{-1}	H-bond	$\pi-\pi$ stacking	hydrophobic contacts (at 5 Å)
[Mn(L)] (1)	−5.836	LYS 116		PRO 117, ILE 181, MET 184, TYR 160, LEU 115, ILE 141, TYR 137, LEU 122
[Ni(L)] (2)	−6.374	LYS 116		ILE 181, MET 184, TYR 160, LEU 115, PRO 117, ILE 141, TYR 137, LEU 122
[Cu(L)] (3)	−5.824	PRO 117		TYR 137, ILE 181, MET 184, TYR 160, LEU 115, PRO 117, ILE 141, LEU 122
[Zn(L)] (4)	−5.711	LYS 116		TYR 160, ILE 181, MET 184, LEU 115, PRO 117, ILE 141, TYR 137, LEU 122
[Mn(L)(bpy)](5)	−5.382	GLU 140	LYS 136	PHE 133, TYR 137, ILE 141, LEU122, TYR 160, PRO 117, LEU 115, PRO 113
[Ni(L)(bpy)] (6)	−5.643	GLU 140	LYS 136	PRO 113, PHE 133, TYR 137, ILE 141, LEU122, TYR 160, PRO 117, LEU 115
[Cu(L)(bpy)] (7)	−6.856	GLU 140	LYS 136	PRO 113, PHE 133, TYR 137, ILE 141, LEU122, TYR 160, PRO 117, LEU 115
[Zn(L)(bpy)] (8)	−5.471	GLU 140	LYS 136	TYR 137, PRO 113, PHE 133, ILE 141, LEU 122, TYR 160, PRO 117, LEU 115

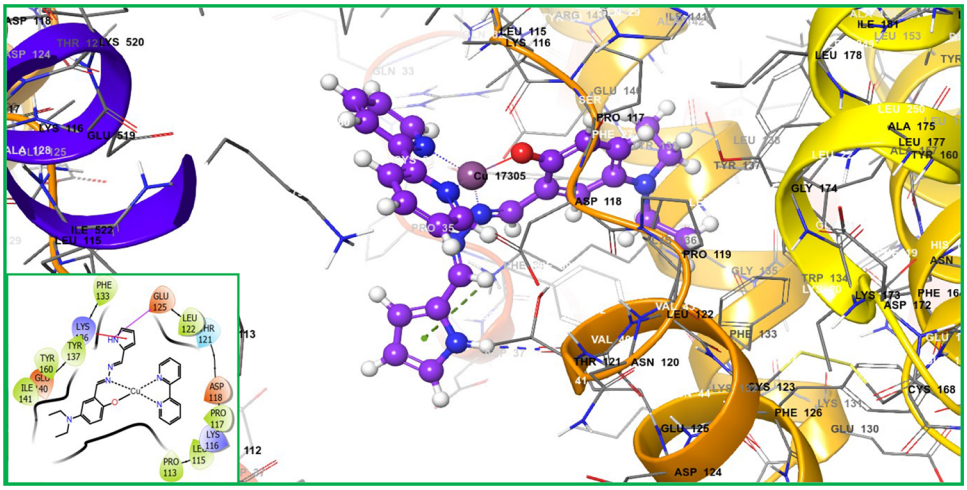

Figure 10. 3D and 2D interaction of the [Cu(L)(bpy)]complex (7) located in hydrophobic sites of receptor BSA.

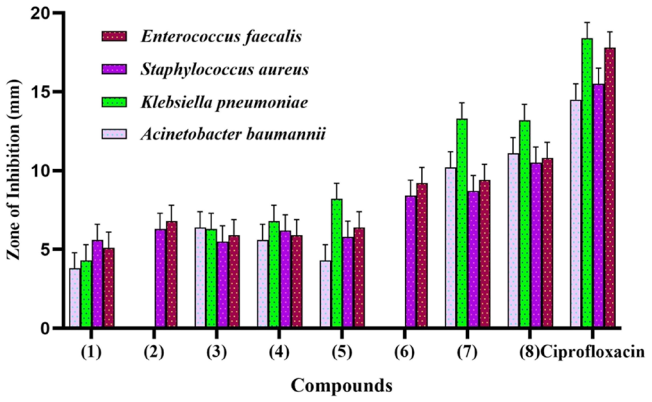

Figure 11. Antibacterial activity of metal(II) complexes (1−8) tested against pathogens by a disc diffusion method.

From the binding affinity results, all the complexes effectively bind with the active site of the BSA receptor. When the docking score value was more negative, the binding nature of a complex with the receptor was greater. Therefore, the metal(II) complexes strongly regulate BSA in therapeutic strategies and cancer prevention.

The in vitro antibacterial assay of metal(II) complexes was tested against *Enterococcus faecalis*, *Staphylococcus aureus*, *Klebsiella pneumonia*, and *Acinetobacter baumannii* pathogens.[24,37] The zone of inhibition was measured for prepared complexes by the disc diffusion method, and their observation revealed that the complexes had significant antibacterial activity, as described in Figure 11, and their inhibition diameters are depicted in Table 5.

In this series, the mixed ligand copper(II) complex was found to be highly vulnerable than the other complexes. These results are very much consistent with molecular docking results, and these values are very close to the standard drug

https://doi.org/10.1021/acsomega.3c02860
ACS Omega 2023, 8, 34458−34470

Table 5. Antibacterial Activity of Metal(II) Complexes (1−8) against Pathogenic Bacteria Tested by a Disc Diffusion Method

	inhibition zone measured (mm)			
complexes	*Enterococcus faecalis*	*Staphylococcus aureus*	*Klebsiella pneumoniae*	***Acinetobacter baumannii***
[Mn(L)] (1)	5.1 ± 0.5	5.6 ± 0.5	4.3 ± 0.5	3.8 ± 0.5
[Ni(L)] (2)	6.8 ± 0.5	6.3 ± 0.5		
[Cu(L)] (3)	5.9 ± 0.5	5.5 ± 0.5	6.3 ± 0.5	6.4 ± 0.5
[Zn(L)] (4)	5.9 ± 0.5	6.2 ± 0.5	6.8 ± 0.5	5.6 ± 0.5
[Mn(L)(bpy)] (5)	6.4 ± 0.5	5,8 ± 0.5	8.2 ± 0.5	4.3 ± 0.5
[Ni(L)(bpy)] (6)	9.2 ± 0.5	8.4 ± 0.5		
[Cu(L)(bpy)] (7)	10.8 ± 0.5	10.5 ± 0.5	13.3 ± 0.5	11.1 ± 0.5
[Zn(L)(bpy)] (8)	9.4 ± 0.5	8.7 ± 0.5	13.2 ± 0.5	10.2 ± 0.5
ciprofloxacin	17.8 ± 0.5	15.5 ± 0.5	18.4 ± 0.5	14.5 ± 0.5

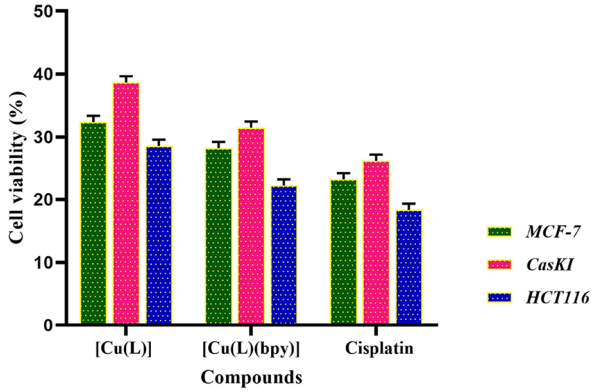

Figure 12. In vitro anticancer activity of copper(II) complexes [Cu(L) (3) & [Cu(L)(bpy) (7) against MCF-7, CaSki, and HCT 116 cancer cell lines.

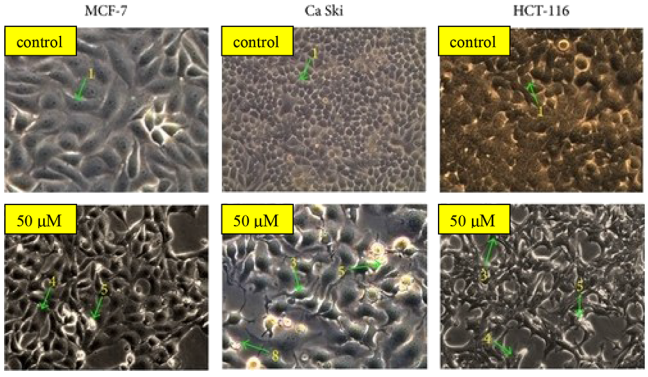

Figure 13. MTT-based antiproliferative photomicrographs of complex (7) on MCF, CaSki, and HCT116 cancer cell lines after 24 h incubation under the phase contrast microscope. Arrows indicate (1) control cell, (2) condensed nuclei, (3) cell shrinkage, (4) membrane blebbing, and (5) apoptotic bodies.

ciprofloxacin. Zone of inhibition measurement for complex (7) shows 10.8 ± 0.5, 10.5 ± 0.5, 13.3 ± 0, and 11.1 ± 0.5 mm, corresponding to *Enterococcus faecalis*, *Staphylococcus aureus*, *Klebsiella pneumoniae*, and *Acinetobacter baumannii*, respectively. The complexes were more potent only at increasing in concentration on all the tested bacterium as explained in Tweedy's chelation theory.[34] On comparison of pathogens against the tested metal(II) complexes, *Klebsiella pneumoniae* showed the highest inhibition with complex (7). Particularly, the presence of bio-significant copper(II) metal ions and aromatic bipyridyl (potential intercalator) moieties provide the complexes with the opportunity to insert into the grooves of the double-helical DNA causing damage.[36] This enhancement in activity suggests that chelation moderately increased the lipophilic character of the compounds and subsequently their permeation through the lipid layer of the microbe's cell membrane.

MTT assay was used to examine the toxicity of Cu(II) (3) and (7).[38] The increasing concentrations promote the anti-proliferation of the human colon cancer cell line HCT116, the human cervical epidermoid carcinoma CaSki, and the human breast cancer cell line MCF7, as indicated in Figure 12 and Table 6. At initial concentrations of 6.25 μg/mL, the complexes showed lower cytotoxicity over death of cancerous cells and upon increased concentration showed better activity against MCF7, CaSki, and HCT116 cells. The IC_{50} values for complex (7) are 28.21 ± 0.72 μM, 31.44 ± 0.72 μM, and 22.19 ± 0.72 μM against the MCF7 human breast adenocarcinoma cell line, CaSki human caucasian cervical epidermoid carcinoma, and HCT116 human colon, respectively.[39,40] It is relative to the bipyridyl moiety in the synthesized copper(II) complexes (7) which exhibited better cytotoxic activity against *MCF-7*, *CaSki*, and *HCT116* than the 1:1 stoichiometric Cu(II) complex (3).

The photomicrographs showed a variety of cytotoxic forms, including condensed nuclei, cell shrinkage, membrane blebbing, bubbling, and echinoid spikes (Figure 13). It is

Table 6. In Vitro Anticancer Activity of Copper(II) Complexes (3) and (7) against MCF-7 and CaSki

		cell lines tested IC_{50} (μM)[a]		
s. no	complexes	*MCF-7*	*CaSki*	*HCT116*
1	**[Cu(L)] (3)**	32.35 ± 0.72	38.62 ± 0.72	28.55 ± 0.72
2	**[Cu(L)(bpy)] (7)**	28.21 ± 0.72	31.44 ± 0.72	22.19 ± 0.72
3	**cisplatin**	23.19 ± 0.72	26.13 ± 0.72	18.32 ± 0.72
4	**control**	100	100	100

[a]Average of three independent determinations.

https://doi.org/10.1021/acsomega.3c02860
ACS Omega 2023, 8, 34458−34470

Table 7. Antioxidant Activity of Ligands and Metal Complexes (1−8) at Different Concentrations Using DPPH Assay

	concentration (μg/mL)											
complexes	0	10	20	30	40	50	60	70	80	90	100	IC_{50} (μg/mL)
[Mn(L)] (1)	0	3.51	5.11	8.3	13.09	18.53	28.75	35.21	48.88	58.45	64.58	83.376
[Ni(L)] (2)	0	2.32	3.72	13.95	14.88	28.37	34.88	40.01	44.18	49.3	56.57	88.411
[Cu(L)] (3)	0	0.15	6.12	16.37	25.82	38.3	45.6	46.88	50.94	50.53	56.86	71.594
[Zn(L)] (4)	0	1.52	6.28	10.47	21.46	27.74	36.82	40.31	46.17	53.66	60.47	83.044
[Mn(L)(bpy)](5)	0	6.73	22.47	32.77	33.16	39.02	47.41	54.21	57.04	62.24	68.24	66.323
[Ni(L)(bpy)] (6)	0	0.57	6.87	17.47	26.36	39.25	46.41	49.28	52.14	52.43	59.31	68.621
[Cu(L)(bpy)] (7)	0	22.09	28.4	34.71	43.88	49.58	51.62	54.47	55.69	59.56	65.26	55.400
[Zn(L)(bpy)] (8)	0	20.76	26.74	32.7	42.43	47.72	49.9	51.16	53.58	56.75	61.9	64.354

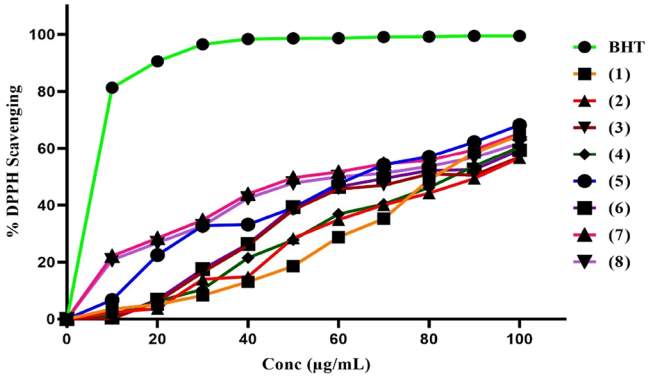

Figure 14. Graphical representation of % DPPH scavenging of metal complexes (1−8) with respect to standard (BHT).

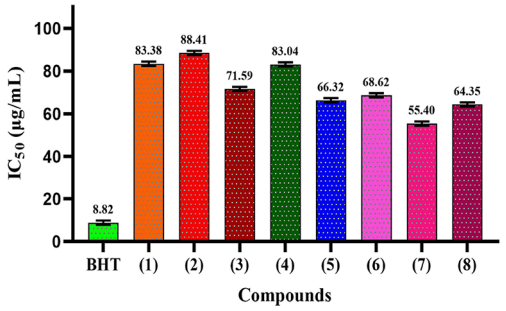

Figure 15. Comparative IC_{50} values of DPPH scavenging of metal complexes (1−8) with respect to standard (BHT).

evident that complex (7) interacts strongly hydrophobically with both DNA and protein, which increases their activity. The cytotoxic potency of the copper(II) complex was very much consistent with the molecular docking results.

The anti-oxidant activity and IC50 values of complexes in methanolic solutions at different concentrations are displayed in Table 7. The findings indicate that the scavenging action of these compounds was concentration-dependent. In this series, the complex [Cu(L)(bpy)] (7) showed a significant capacity for interaction with DPPH, which was concentration dependent, and this compound expressed an IC_{50} value of 55.40 μg/mL inferior than other stoichiometric complexes.[41] Moreover, the results of complex's antioxidant activity are compared to BHT (8.8153 μg/mL) as the reference standard control and described in Figures 14 and 15. Maximum free radical scavenging activity of complex (7) was due to biological active Cu(II) metal ions coordinated with bipyridyl ligands.

4. CONCLUSIONS

In conclusion, eight novel azine Schiff-base ligands have been created along with their Mn(II), Ni(II), Cu(II), and Zn(II) complexes. Various spectroscopic techniques were used to describe all of these complexes and ligands. The ligands preferentially attach to the metal in an OH manner with salicylaldehyde and one nitrogen atom from an azine. Regardless of the molar ratio of the metal to ligand, our attempt to produce 1:1 and mixed ligand complexes with NN (bpy) and NO bonding was successful. The anticancer and antibacterial activity of the complexes in vitro showed their potency; however, complex (7) was shown to be the most effective among all the compounds. The complex [Cu(L)-(bpy)] demonstrated a significant concentration-dependent interaction with DPPH in this series, and this compound displayed a lower IC50 value of 110.11 μM than other stoichiometric compounds. According to theoretical studies, Cu(II) complexes are more reactive than other complexes due to their smaller HOMO−LUMO energy gap. The molecular docking investigation also helped to comprehend and pinpoint the location of the Cu(II) complex's active site in relation to the BSA receptor.

■ ASSOCIATED CONTENT

Supporting Information

The Supporting Information is available free of charge at https://pubs.acs.org/doi/10.1021/acsomega.3c02860.

Scheme of ligand synthesis (HL); C^{13} NMR spectrum of ligand (HL); ^{1}H NMR spectrum of Zn metal complex (8); C^{13} NMR spectrum of Zn metal complex (8); geometry parameters of metal(II) complexes (1−8) by the B3LYP method using the LACVP++ basis set; and optimized molecular structure of metal(II) complexes 1−8 (PDF)

■ AUTHOR INFORMATION

Corresponding Authors

Annadurai Subramani − *Department of Biochemistry, Dwaraka Doss Goverdhan Doss Vaishnav College, Chennai 600106 Tamil Nadu, India*; Email: subuchem71@gmail.com

Mustafa K. A. Mohammed − *University of Warith Al-Anbiyaa, 56001 Karbala, Iraq*; orcid.org/0000-0002-1850-6355; Email: mustafa_kareem97@yhaoo.com

Syed J. Askar Ali − *Post-Graduate and Research Department of Chemistry, the New College (Autonomous), Chennai 600014, India*; Email: sjaaresearchgroup@gmail.com

https://doi.org/10.1021/acsomega.3c02860
ACS Omega 2023, 8, 34458−34470

Sasikumar Ponnusamy − *Department of Physics, Saveetha School of Engineering, SIMATS, Chennai 602 701, India*; Email: sasijanaki123@gmail.com

Authors

Sivan Arulmozhi − *Post-Graduate and Research Department of Chemistry, the New College (Autonomous), Chennai 600014, India*

Gopalakrishnan Sasikumar − *Department of Chemistry, St. Joseph's College of Engineering, OMR, Chennai 600 119, India*

Majid S. Jabir − *Department of Applied Sciences, University of Technology-Iraq, 10011 Baghdad, Iraq*; orcid.org/0000-0003-0759-8298

Abdallah M. Elgorban − *Department of Botany and Microbiology, College of Science, King Saud University, Riyadh 11451, Saudi Arabia*

Wanli Zhang − *School of Food Science and Engineering, Hainan University, Haikou 570228, PR China*

Hema Natarajan − *Department of Physics, Jerusalem College of Engineering, Chennai 600100, India*

Complete contact information is available at: https://pubs.acs.org/10.1021/acsomega.3c02860

Notes

The authors declare no competing financial interest.

■ ACKNOWLEDGMENTS

The authors extend their appreciation to the Researchers Supporting Project number (RSP2023R56), King Saud University, Riyadh, Saudi Arabia.

■ REFERENCES

(1) More, M.; Joshi, P.; Mishra, Y.; Khanna, P. Metal complexes driven from Schiff bases and semicarbazones for biomedical and allied applications: a review. *Mater. Today Chem.* **2019**, *14*, No. 100195.

(2) Riyazahmed, K. S.; Bora, D.; Shankaraiah, N. Application of Transition Metal-Catalyzed C− H Activation Strategies in the Synthesis and Functionalization of β-Carbolines. *Asian J. Org. Chem.* **2021**, *10*, 1050−1066.

(3) Chen, R.; Shi, J. L.; Ma, Y.; Lin, G.; Lang, X.; Wang, C. Designed Synthesis of a 2D Porphyrin-Based sp2 Carbon-Conjugated Covalent Organic Framework for Heterogeneous Photocatalysis. *Angew. Chem., Int. Ed.* **2019**, *58*, 6430−6434.

(4) Pervaiz, M.; Sadiq, S.; Sadiq, A.; Younas, U.; Ashraf, A.; Saeed, Z.; Zuber, M.; Adnan, A. Azo-Schiff base derivatives of transition metal complexes as antimicrobial agents. *Coord. Chem. Rev.* **2021**, *447*, No. 214128.

(5) Radha, V. P.; Prabakaran, M. Novel thiadiazole-derived Schiff base ligand and its transition metal complexes: Thermal behaviour, theoretical study, chemo-sensor, antimicrobial, antidiabetic and anticancer activity. *Appl. Organomet. Chem.* **2022**, *36*, No. e6872.

(6) Kar, S.; Milstein, D. Sustainable catalysis with fluxional acridine-based PNP pincer complexes. *Chem. Commun.* **2022**, *58*, 3731−3746.

(7) Qi, M.-Y.; Conte, M.; Anpo, M.; Tang, Z.-R.; Xu, Y.-J. Cooperative coupling of oxidative organic synthesis and hydrogen production over semiconductor-based photocatalysts. *Chem. Rev.* **2021**, *121*, 13051−13085.

(8) Liu, Y.; Lu, F.; Xu, N.; Wang, B.; Yang, L.; Huang, Y.; Hu, Z. Mechanically robust, hydrothermal aging resistant, imine-containing epoxy thermoset for recyclable carbon fiber reinforced composites. *Mater. Des.* **2022**, *224*, No. 111357.

(9) O'Malley, D. P.; Li, K.; Maue, M.; Zografos, A. L.; Baran, P. S. Total synthesis of dimeric pyrrole− imidazole alkaloids: Sceptrin, Ageliferin, Nagelamide E, Oxysceptrin, Nakamuric acid, and the Axinellamine carbon skeleton. *J. Am. Chem. Soc.* **2007**, *129*, 4762−4775.

(10) Bellina, F.; Rossi, R. Synthesis and biological activity of pyrrole, pyrroline and pyrrolidine derivatives with two aryl groups on adjacent positions. *Tetrahedron* **2006**, *62*, 7213−7256.

(11) Khashi, M.; Davoodnia, A.; Prasada Rao Lingam, V. DMAP catalyzed synthesis of some new pyrrolo [3, 2-e][1, 2, 4] triazolo [1, 5-c] pyrimidines. *Res. Chem. Intermed.* **2015**, *41*, 5731−5742.

(12) Mosquera, A.; Riveiros, R.; Sestelo, J. P.; Sarandeses, L. A. Cross-coupling reactions of indium organometallics with 2, 5-dihalopyrimidines: synthesis of hyrtinadine A. *Org. Lett.* **2008**, *10*, 3745−3748.

(13) Cai, X.-H.; Tan, Q.-G.; Liu, Y.-P.; Feng, T.; Du, Z.-Z.; Li, W.-Q.; Luo, X.-D. A cage-monoterpene indole alkaloid from Alstonia scholaris. *Org. Lett.* **2008**, *10*, 577−580.

(14) Garg, N. K.; Sarpong, R.; Stoltz, B. M. The first total synthesis of dragmacidin D. *J. Am. Chem. Soc.* **2002**, *124*, 13179−13184.

(15) Kivelson, D.; Neiman, R. ESR studies on the bonding in copper complexes. *J. Chem. Phys.* **1961**, *35*, 149−155.

(16) Aggoun, D.; Messasma, Z.; Bouzerafa, B.; Berenguer, R.; Morallon, E.; Ouennoughi, Y.; Ourari, A. Synthesis, characterization and DFT investigation of new metal complexes of Ni (II), Mn (II) and VO (IV) containing N, O-donor Schiff base ligand. *J. Mol. Struct.* **2021**, *1231*, No. 129923.

(17) Bauer, A. W.; Perry, D. M.; Kirby, W. M. Drug usage and antibiotic susceptibility of staphylococci. *J. Am. Med. Assoc.* **1960**, *173*, 475−480.

(18) Pagning, A. L. N.; Lateef, M.; Tapondjou, L. A.; Kuiate, J.-R.; Ngnokam, D.; Ali, M. S. New triterpene and new flavone glucoside from Rhynchospora corymbosa (Cyperaceae) with their antimicrobial, tyrosinase and butyrylcholinesterase inhibitory activities. *Phytochem. Lett.* **2016**, *16*, 121−128.

(19) Munira, M.; Uddin, M.; Islam, M.; Aktar, K.; Muhit, A. Evaluation of antioxidant, cytotoxic, antibacterial and thrombolytic activity of the methanolic extracts of Ficus racemosa fruits. *J. Complementary Altern. Med. Res.* **2018**, *5*, 1−13.

(20) Bochevarov, A. D.; Harder, E.; Hughes, T. F.; Greenwood, J. R.; Braden, D. A.; Philipp, D. M.; Rinaldo, D.; Halls, M. D.; Zhang, J.; Friesner, R. A. Jaguar: A high-performance quantum chemistry software program with strengths in life and materials sciences. *Int. J. Quantum Chem.* **2013**, *113*, 2110−2142.

(21) El-Sonbati, A.; Diab, M.; El-Bindary, A.; Eldesoky, A.; Morgan, S. M. Correlation between ionic radii of metals and thermal decomposition of supramolecular structure of azodye complexes. *Spectrochim. Acta, Part A* **2015**, *135*, 774−791.

(22) Friesner, R. A.; Murphy, R. B.; Repasky, M. P.; Frye, L. L.; Greenwood, J. R.; Halgren, T. A.; Sanschagrin, P. C.; Mainz, D. T. Extra precision glide: Docking and scoring incorporating a model of hydrophobic enclosure for protein− ligand complexes. *J. Med. Chem.* **2006**, *49*, 6177−6196.

(23) Shu, Y.; Xue, W.; Xu, X.; Jia, Z.; Yao, X.; Liu, S.; Liu, L. Interaction of erucic acid with bovine serum albumin using a multi-spectroscopic method and molecular docking technique. *Food Chem.* **2015**, *173*, 31−37.

(24) Alyamani, A. A.; Al-Musawi, M. H.; Albukhaty, S.; Sulaiman, G. M.; Ibrahim, K. M.; Ahmed, E. M.; Jabir, M. S.; Al-Karagoly, H.; Aljahmany, A. A.; Mohammed, M. K. Electrospun Polycaprolactone/Chitosan Nanofibers Containing Cordia myxa Fruit Extract as Potential Biocompatible Antibacterial Wound Dressings. *Molecules* **2023**, *28*, 2501.

(25) Naji, A. M.; Mohammed, I. Y.; Mohammed, S. H.; Mohammed, M. K.; Ahmed, D. S.; Jabir, M. S.; Rheima, A. M. Photocatalytic degradation of methylene blue dye using F doped ZnO/polyvinyl alcohol nanocomposites. *Mater. Lett.* **2022**, *322*, No. 132473.

(26) Majeed, S. M.; Mohammed, M. K.; Ahmed, D. S. Efficient and hysteresis-free mixed-dimensional 2D/3D perovskite solar cells using ethyl lactate as a green additive to perovskite precursor solutions. *J. Mater. Chem. C* **2022**, *10*, 16480−16491.

(27) Lupaşcu, G.; Pahonţu, E.; Shova, S.; Bărbuceanu, Ş. F.; Badea, M.; Paraschivescu, C.; Neamţu, J.; Dinu, M.; Ancuceanu, R. V.; Drăgănescu, D. Co (II), Cu (II), Mn (II), Ni (II), Pd (II), and Pt (II) complexes of bidentate Schiff base ligand: Synthesis, crystal structure, and acute toxicity evaluation. *Appl. Organomet. Chem.* **2021**, *35*, No. e6149.
(28) Ravichandran, J.; Gurumoorthy, P.; Karthick, C.; Rahiman, A. K. Mononuclear zinc (II) complexes of 2-((2-(piperazin-1-yl) ethylimino) methyl)-4-substituted phenols: Synthesis, structural characterization, DNA binding and cheminuclease activities. *J. Mol. Struct.* **2014**, *1062*, 147−157.
(29) Bindu, P.; Kurup, M. R. P.; Satyakeerty, T. R. Epr, cyclic voltammetric and biological activities of copper (II) complexes of salicylaldehyde N (4)-substituted thiosemicarbazone and heterocyclic bases. *Polyhedron* **1998**, *18*, 321−331.
(30) Hathaway, B.; Billing, D. The electronic properties and stereochemistry of mono-nuclear complexes of the copper (II) ion. *Coord. Chem. Rev.* **1970**, *5*, 143−207.
(31) Sasikumar, G.; Arulmozhi, S.; Ashma, A.; Sudha, A.; Askar ali, S. J. Mixed ligand ternary complexes of Co (II), Ni (II), Cu (II) and Zn (II) and their structural characterization, electrochemical, theoretical and biological studies. *J. Mol. Struct.* **2019**, *1187*, 108−120.
(32) Al-Mousoi, A. K.; Mohammed, M. K.; Khalaf, H. A. Preparing and characterization of indium arsenide (InAs) thin films by chemical spray pyrolysis (CSP) technique. *Optik* **2016**, *127*, 5834−5840.
(33) Dastan, D.; Jafari, A.; Marszalek, T.; Mohammed, M. K.; Tao, L.; Shi, Z.; Chen, Y.; Yin, X.-T.; Alharbi, N. D.; Gity, F. Influence of heat treatment on H2S gas sensing features of NiO thin films deposited via thermal evaporation technique. *Mater. Sci. Semicond. Process.* **2023**, *154*, No. 107232.
(34) Al Rugaie, O.; Jabir, M. S.; Mohammed, M. K.; Abbas, R. H.; Ahmed, D. S.; Sulaiman, G. M.; Mohammed, S. A.; Khan, R. A.; Al-Regaiey, K. A.; Alsharidah, M. Modification of SWCNTs with hybrid materials ZnO−Ag and ZnO−Au for enhancing bactericidal activity of phagocytic cells against Escherichia coli through NOX2 pathway. *Sci. Rep.* **2022**, *12*, 17203.
(35) Taslimi, P.; Türkan, F.; Güngördü Solğun, D.; Aras, A.; Erden, Y.; Celebioglu, H. U.; Tuzun, B.; Ağırtaş, M. S.; Günay, S.; Gulcin, I. Metal contained Phthalocyanines with 3, 4-Dimethoxyphenethoxy substituents: their anticancer, antibacterial activities and their inhibitory effects on some metabolic enzymes with molecular docking studies. *J. Biomol. Struct. Dyn.* **2022**, *40*, 2991−3002.
(36) Ji, L.-N.; Zou, X.-H.; Liu, J.-G. Shape-and enantioselective interaction of Ru (II)/Co (III) polypyridyl complexes with DNA. *Coord. Chem. Rev.* **2001**, *216*, 513−536.
(37) Ahmed, D. S.; Mohammed, M. K. Studying the bactericidal ability and biocompatibility of gold and gold oxide nanoparticles decorating on multi-wall carbon nanotubes. *Chem. Pap.* **2020**, *74*, 4033−4046.
(38) Mahmood, R. I.; Kadhim, A. A.; Ibraheem, S.; Albukhaty, S.; Mohammed-Salih, H. S.; Abbas, R. H.; Jabir, M. S.; Mohammed, M. K.; Nayef, U. M.; AlMalki, F. A.; Sulaiman, G. M.; al-Karagoly, H. Biosynthesis of copper oxide nanoparticles mediated Annona muricata as cytotoxic and apoptosis inducer factor in breast cancer cell lines. *Sci. Rep.* **2022**, *12*, 16165.
(39) Sasikumar, G.; Subramani, A.; Tamilarasan, R.; Rajesh, P.; Sasikumar, P.; Albukhaty, S.; Mohammed, M. K.; Karthikeyan, S.; Al-Aqbi, Z. T.; Al-Doghachi, F. A. Catalytic, Theoretical, and Biological Investigations of Ternary Metal (II) Complexes Derived from L-Valine-Based Schiff Bases and Heterocyclic Bases. *Molecules* **2023**, *28*, 2931.
(40) Tamilarasan, R.; Subramani, A.; Sasikumar, G.; Ganapathi, P.; Karthikeyan, S.; Ponnusamy, S.; Albukhaty, S.; Mohammed, M. K.; Al-Aqbi, Z. T.; Al-Doghachi, F. A. Catalytic response and molecular simulation studies in the development of synthetic routes in trimeric triaryl pyridinium type ionic liquids. *Sci. Rep.* **2023**, *13*, 4453.
(41) Gabrielska, J.; Soczyńska-Kordala, M.; Hładyszowski, J.; Żyłka, R.; Miśkiewicz, J.; Przestalski, S. Antioxidative effect of quercetin and its equimolar mixtures with phenyltin compounds on liposome membranes. *J. Agric. Food Chem.* **2006**, *54*, 7735−7746.

https://doi.org/10.1021/acsomega.3c02860
ACS Omega 2023, 8, 34458−34470